European Journal of Radiology 118 (2019) 187–193

Contents lists available at ScienceDirect

European Journal of Radiology

journal homepage: www.elsevier.com/locate/ejrad

Research article

# The enhanced $T_2$ star weighted angiography (ESWAN) value for differentiating borderline from malignant epithelial ovarian tumors

Xu Han[a], Meiyu Sun[a,*], Mengyao Wang[a], Rui Fan[a], Dan Chen[b], Lizhi Xie[c], Ailian Liu[a]

[a] Department of Radiology, The First Affiliated Hospital of Dalian Medical University, Dalian, Liaoning, China
[b] Department of Pathology, The First Affiliated Hospital of Dalian Medical University, Dalian, Liaoning, China
[c] GE Healthcare, MR Research China, Beijing, China

ARTICLE INFO

*Keywords:*
ESWAN
$R_2$* value
Epithelial ovarian cancer
Borderline
Malignant

ABSTRACT

*Purpose:* To investigate the potential of ESWAN in differentiating borderline epithelial ovarian tumors (BEOTs) from malignant epithelial ovarian tumors (MEOTs).

*Method:* Thirty-four patients with 37 lesions were enrolled, including 14 BEOTs and 23 MEOTs. The magnitude, phase, $R_2$* and $T_2$* maps were analyzed by two observers. The regions of interest were drawn along the boundaries of tumors on the slice with maximal solid area, according to fat suppression $T_2$WI and $T_1$WI. The consistency among the three measurements taken by two observers was tested by intra-class correlation coefficients. Agreement of average values measured by two observers was evaluated by Bland-Altman plots. All the data of BEOTs and MEOTs were compared using the independent-sample *t* test. The receiver operating characteristic curve was used to evaluate the diagnostic performance.

*Results:* No statistical differences were observed in the magnitude and phase values between two tumor groups. The $R_2$* value of BEOTs was lower than that of MEOTs ($P < 0.001$), whereas the $T_2$* value of BEOTs was higher than that of MEOTs ($P = 0.01$). The area under the curve of $R_2$* values was 0.894 and the corresponding cutoff value was 7.50 Hz, with the sensitivity, specificity and accuracy of 85.7%, 82.6% and 86.5%, respectively. The AUC of $T_2$* values was 0.776 and the corresponding cutoff value was 143.73 ms with the sensitivity, specificity and accuracy of 71.4%, 82.6% and 78.4%, respectively.

*Conclusions:* $R_2$* and $T_2$* values can be used for quantificationally differentiating BEOTs from MEOTs and the $R_2$* has better diagnostic performance.

## 1. Introduction

Epithelial ovarian cancer (EOC) is the second leading cause of death in gynecological cancer worldwide and accounts for approximately 90% of all ovarian cancers [1,2]. EOCs can be classified into borderline and malignant epithelial tumors depending on the tumor aggressiveness [2]. Borderline epithelial ovarian tumors (BEOTs), also known as low malignant potential tumors, account for approximately 15%–20% of all EOCs [3]. Histologically, BEOTs are characterized by at least 10% of epithelial cells with atypical proliferation, moderate nuclear atypia and active mitosis, no stromal invasion and microinvasion that is found in approximately 10% cases [4,5]. The clinical manifestations and imaging features of BEOTs are similar to those of malignant epithelial ovarian tumors (MEOTs) [6]. However, unlike MEOTs, BEOTs usually occur in young women with an intention to preserve fertility, and they could be treated with fertility sparing surgery [7,8] and carry a favorable prognosis [3]. Accurate preoperative diagnosis is of great significance in deciding the optimal surgical procedure and improving the life quality of patients.

Various laboratory and imaging tests have been used to differentiate BEOTs from MEOTs. Cancer antigen (CA) 125 cannot be used to predict the invasiveness of the tumor due to low diagnostic accuracy and a high risk of false-positive result [9], although CA125 has been widely applied for the preoperative evaluation of ovarian cancer [10]. Ultrasonography has a relatively low specificity and no specific parameters to differentiate BEOTs from MEOTs. Computed tomography (CT) has a limited value in differentiating BEOTs from MEOTs due to the poor soft tissue contrast [6,11]. Contrarily, conventional magnetic resonance imaging (MRI) can clearly reveal the cystic and solid components of tumors on $T_2$-weighted images ($T_2$WI). The MRI features of BEOTs and

* Corresponding author at: No. 222, Zhongshan Road, Xigang District, Dalian City, Liaoning Province, 116011, China.
*E-mail addresses:* hanxudlykdx1206@163.com (X. Han), sunmy828@126.com (M. Sun), 411707879@qq.com (M. Wang), 329739283@qq.com (R. Fan), 18098877136@163.com (D. Chen), rokage@163.com (L. Xie), cjr.liuailian@vip.163.com (A. Liu).

https://doi.org/10.1016/j.ejrad.2019.07.011
Received 24 April 2019; Received in revised form 5 July 2019; Accepted 8 July 2019

**Table 1**
Clinical characteristics and CA125 levels of 34 patients.

| | | BEOTs (n = 14) | MEOTs (n = 20) |
|---|---|---|---|
| Age | | 44.93 (11–68)[a] | 53.80 (35–76)[a] |
| Menstrual | Premenopause | 9 | 6 |
| | Postmenopause | 5 | 14 |
| Location | Unilateral | 14 | 17 |
| | Bilateral | 0 | 3 |
| Histology[b] | Serous | 4 | 14 |
| | Mucous | 7 | 4 |
| | Mixed | 3 | 1 |
| | Endometrioid | 0 | 1 |
| | Clear cell | 0 | 3 |
| FIGO stage | I | 11 | 7 |
| | II | 2 | 4 |
| | III | 1 | 9 |
| | IV | 0 | 0 |
| CA125 | | 27.74 (6.58–167.6)[a] | 386.70 (28.79–1829)[a] |

n presents the number of patients.
[a] Presents average value (range).
[b] Presents the number of tumor lesions(BEOTs 14 lesions, MEOTs 23 lesions).

MEOTs are predominantly cystic masses with solid vegetation or septum. Moreover, MEOTs have larger solid components and thicker septum. Nonetheless, so far no MRI features have been identified as having the ability to differentiate between these two groups of tumors [12].

Enhanced $T_2$ star weighted angiography (ESWAN) is a newly developed technology based on the susceptibility-weighted imaging (SWI). Magnetic susceptibility technology reflects differences of magnetic susceptibility in different tissue, which are determined by the form of iron element in blood [13,14]. The process of tumor proliferation and aggressiveness increases oxygen consumption, which can stimulate the formation of immature neovascularization. The degree of tumor vascularization is positively correlated with the aggressiveness of the tumor, and the formation of immature neovascularization can decrease blood oxygen content as well as increase intratumoral hemorrhage and necrosis [15–17]. Neovascularization and hypoxia are essential factors for tumor progression, which provide a theoretical basis for the use of ESWAN in differentiating BEOTs from MEOTs.

Currently, ESWAN is widely used for the diagnosis of neurological diseases, such as brain tumors, cerebral vascular malformation and diseases, brain injury, neurodegeneration and so on [13,18–20]. With the development of MRI technology, ESWAN has been trying to use for abdominal diseases diagnosis [21–24]. The aim of this study was to investigate the value of ESWAN in differentiating BEOTs from MEOTs.

## 2. Methods and materials

### 2.1. Study population

The Institutional Review Board of our hospital approved this retrospective study, and written informed consent was waived. We retrospectively analyzed the clinical and MR imaging information from patients who underwent ovarian 1.5 T MR examination at our hospital between November 2013 and November 2018. The inclusion criteria were as follows, (1) all subjects were confirmed to have EOCs by pathology; (2) no radiotherapy or chemotherapy was given before the 1.5 T MRI scan; (3) all images without significant artifacts were evaluated by reviewer MYS. Finally, a total of 34 patients with 37 lesions were retrospectively analyzed. All subjects were divided into two groups, including 14 patients (14 lesions) with BEOTs and 20 patients (23 lesions) with MEOTs. Preoperative CA125 levels were obtained for all patients. The clinical characteristics and CA125 levels from 34 patients (37 lesions) are listed in Table 1.

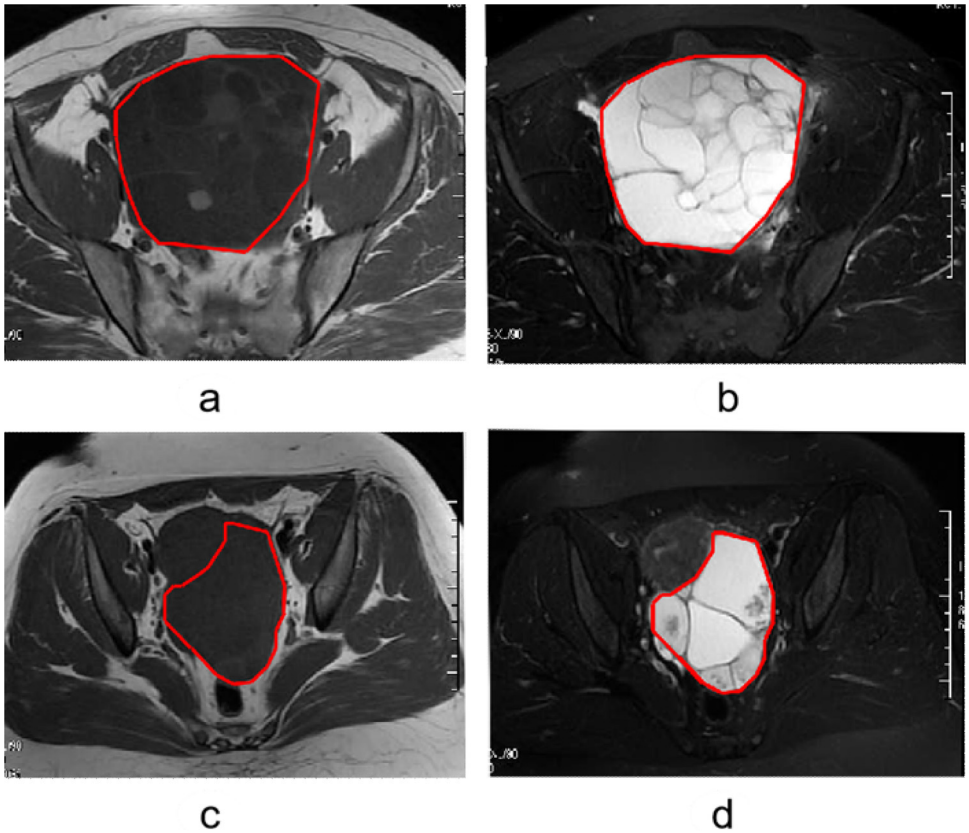


**Fig. 1.** Images show regions of interest (ROIs) were drawn along the edge of tumor on the slice with maximal solid area or maximal slice, according to $T_1$WI (a,c) and fat-suppression $T_2$WI (b,d).

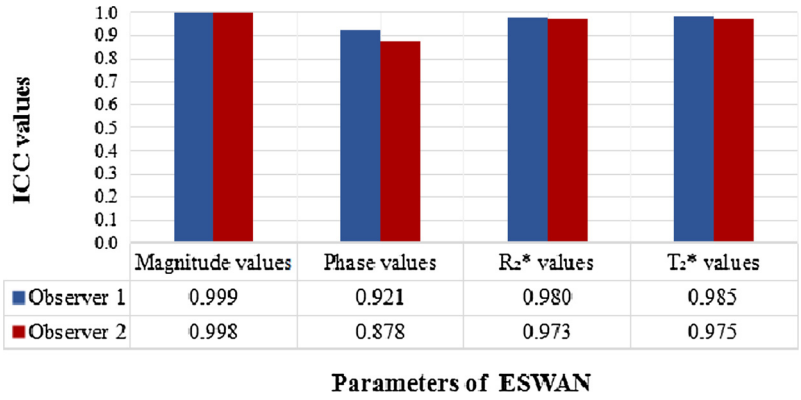


**Fig. 2.** The intra-class agreement of the ESWAN parameters measured by the two observers. The ICC values of the magnitude, phase, $R_2$*, and $T_2$* values were all > 0.75.

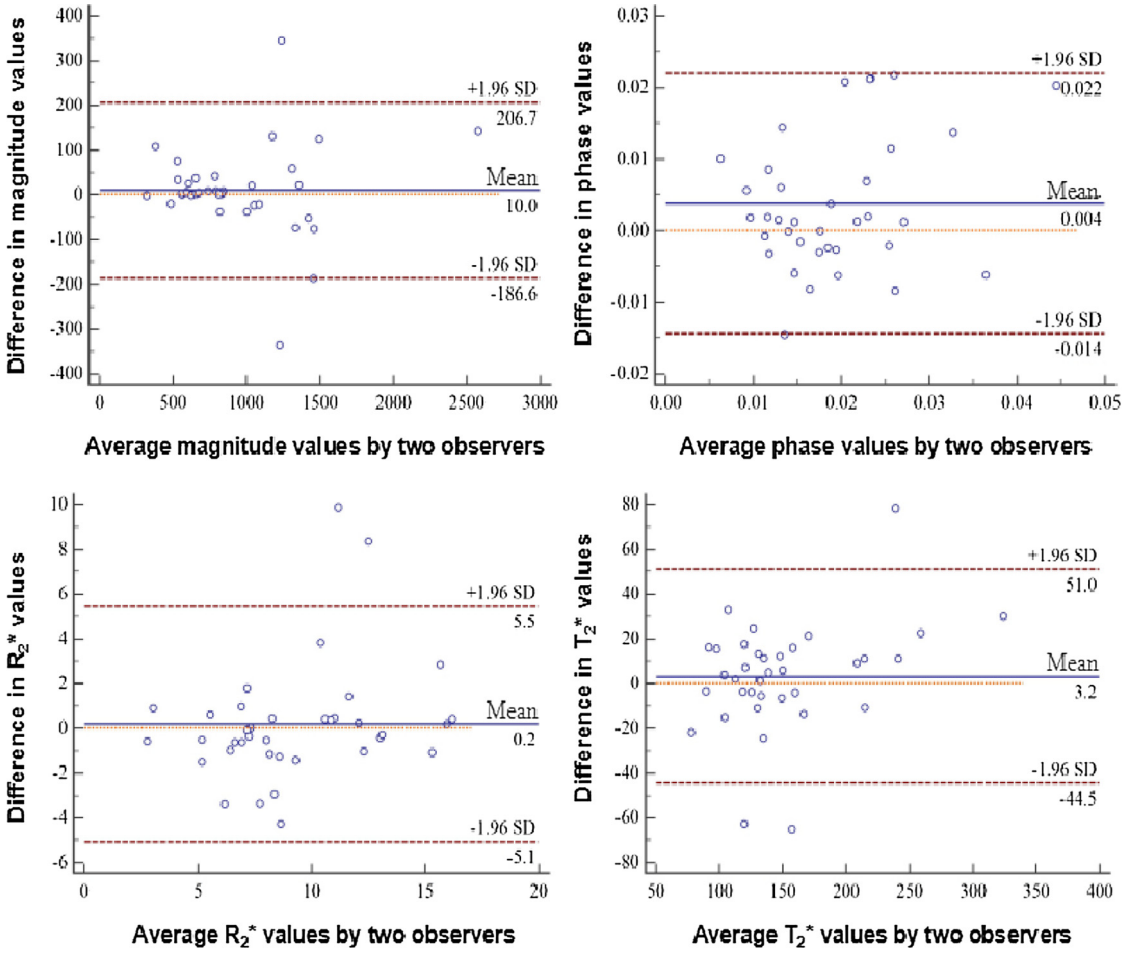


**Fig. 3.** The Bland-Altman plot for evaluating inter-class agreement between different measurements of ESWAN parameters by two observers. A total of 5.41% (2/37) points of magnitude were outside the 95% limits of agreement (LOA); 2.70% (1/37) points of phase were outside the 95% LOA; 5.41% (2/37) points of $R_2$* were outside the 95% LOA rs; 8.11% (3/37) points of $T_2$* were outside the 95% LOA.

**Table 2**
Comparison of ESWAN parameters between BEOTs and MEOTs.

| | BEOTs | MEOTs | *t* | *P* |
|---|---|---|---|---|
| Magnitude (Hz) | 1022.59 ± 583.59 | 901.79 ± 340.78 | 0.80 | 0.43 |
| Phase (ms) | 0.023 ± 0.012 | 0.019 ± 0.008 | 1.20 | 0.24 |
| $R_2$* | 5.98 ± 1.79 | 11.40 ± 3.66 | −6.02 | < 0.001 |
| $T_2$* | 187.91 ± 75.57 | 129.09 ± 28.48 | 2.79 | 0.01 |

### 2.2. Imaging protocol

MRI scans including ESWAN sequences were performed on a 1.5 T scanner (GE Signa HDXT, GE Healthcare, USA) with an 8-channel phased array pelvis coil. $T_1$WI, fat-suppressed $T_2$WI, liver acquisition with volume acceleration (LAVA) and ESWAN were performed for all subjects. The applied imaging parameters were as follows. 1) $T_1$WI. TR = 500 ms, TE = 10 ms, FOV = 36 cm × 36 cm, matrix = 320 × 192, number of excitations (NEX) = 2.0, slice-

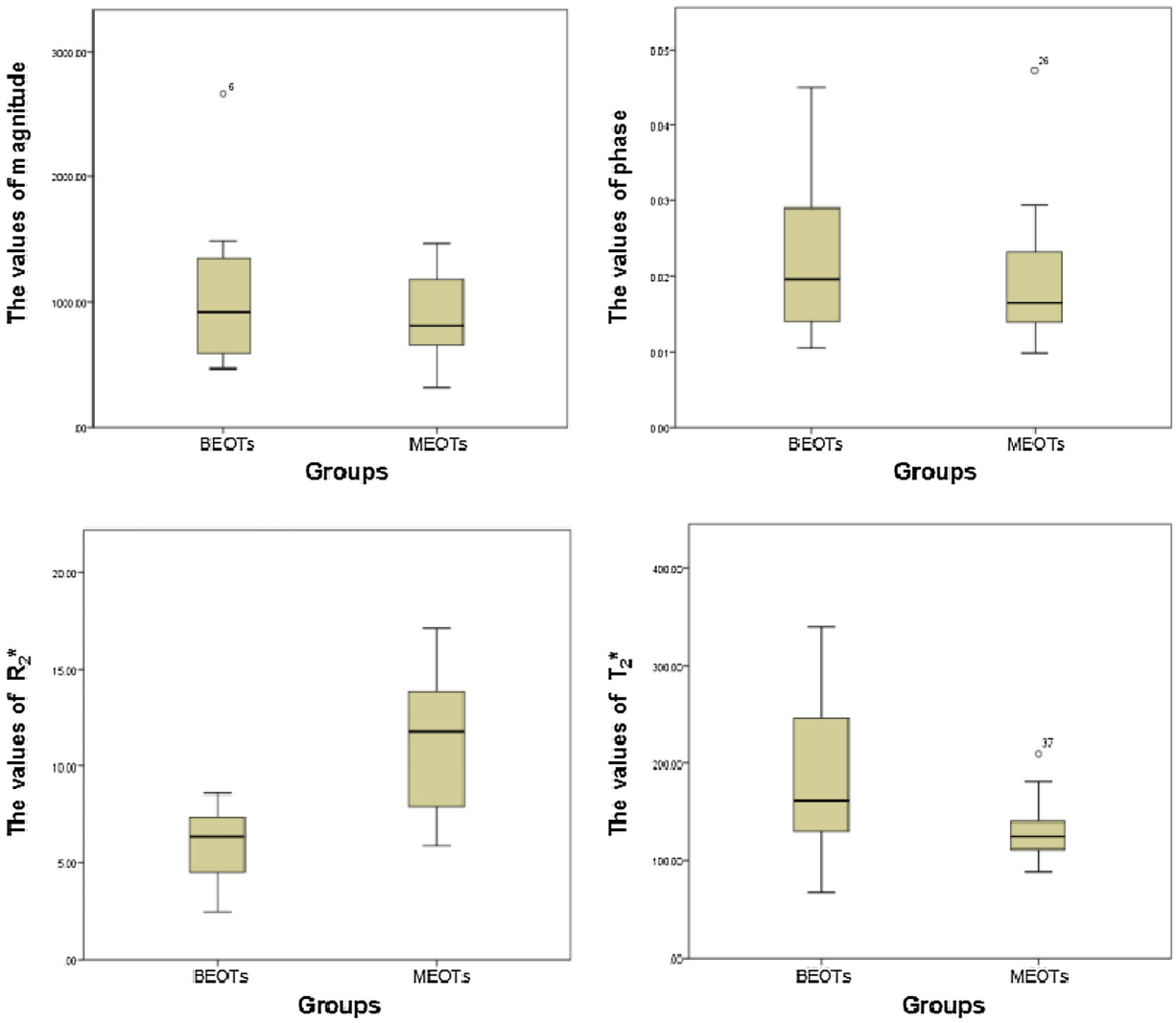


**Fig. 4.** Boxplots show the magnitude, phase, $R_2$*, and $T_2$* values in BEOTs and MEOTs.

thickness = 4 mm, slice-gap = 1 mm; 2) Fat suppression $T_2$. TR = 4000 ms, TE = 125 ms, FOV = 36 cm × 36 cm, matrix = 288 × 224, NEX = 4.0, slice-thickness = 4 mm, slice-gap = 1 mm; 3) LAVA. TR = 3.9 ms, TE = 1.9 ms, FOV = 39 cm × 39 cm, matrix = 272 × 192, NEX = 0.71, flip angle = 12°, slice-thickness = 5.0 mm, slice-gap = 2.5 mm; 4) ESWAN. axial 3D, matrix = 256 × 192, 5 echoes, TR = 16.3 ms, $TE_1$ = 2.1 ms, $TE_2$ = 5.1 ms, $TE_3$ = 8.0 ms, $TE_4$ = 10.9 ms, $TE_5$ = 13.8 ms, flip angle = 12°, bandwidth = ± 62.5 kHz, FOV = 40 cm × 40 cm, slice-thickness = 5 mm, reconstruction thickness = 2 mm, NEX = 0.71, scan matrix = 256 × 192, reconstruction matrix = 512 × 512, parallel acquisitions acceleration factor = 2, breath hold approximately 21 s. Flow compensation was used to obtain continuous axial digital images covering the entire pelvic lesion. In addition, the original magnitude image and original phase image were obtained.

### 2.3. Imaging analysis

The original axial digital images from the ESWAN sequence were transmitted to the GE SDC-ADW 4.6 workstation (Sun Microsystems, Santa Clara, Calif) and the post-processing was performed by Functool software. The magnitude, phase, $R_2$* and $T_2$* maps were automatically constructed, and were reviewed by two observers who were blinded to clinical information and histopathologic results with 18 and 6 years of experience in pelvic imaging, respectively. The manual regions of interest (ROIs) were drawn along the edge of tumors on the slice with maximal solid area (we choose the maximal slice if no solid component or the solid component was too small in tumors), according to fat-suppression $T_2$WI and $T_1$WI (Fig. 1). To assess the intra-observer agreement of the ESWAN parameters, the measurement was repeated for three times, and the averages of three measurements were calculated.

### 2.4. Statistical analysis

Statistical analysis was performed using a SPSS 22.0 statistical software (IBM Corp. Armonk, NY, USA), unless otherwise specified. The Kolmogorov-Smirnov test was used to evaluate whether the data conformed to Gaussian distribution. Data that followed Gaussian distribution were presented as mean ± standard deviation (SD) for continuous variables (such as age, CA125 level, magnitude value, phase value, $R_2$* value and $T_2$* value) and frequencies for categorical variables. A $P < 0.05$ was considered as statistically significant.

The consistency of results measured by two observers was tested by intra-class correlation coefficients (ICC). The ICC values greater than 0.75, between 0.50 and 0.75, and less than 0.50 indicated good concordance, moderate concordance, and poor concordance, respectively. Bland-Altman plots (MedCalc 15.2.2, MedCalc Software bvba, Ostend, Belgium) were provided to evaluate the inter-class agreement of average values measured by two observers.

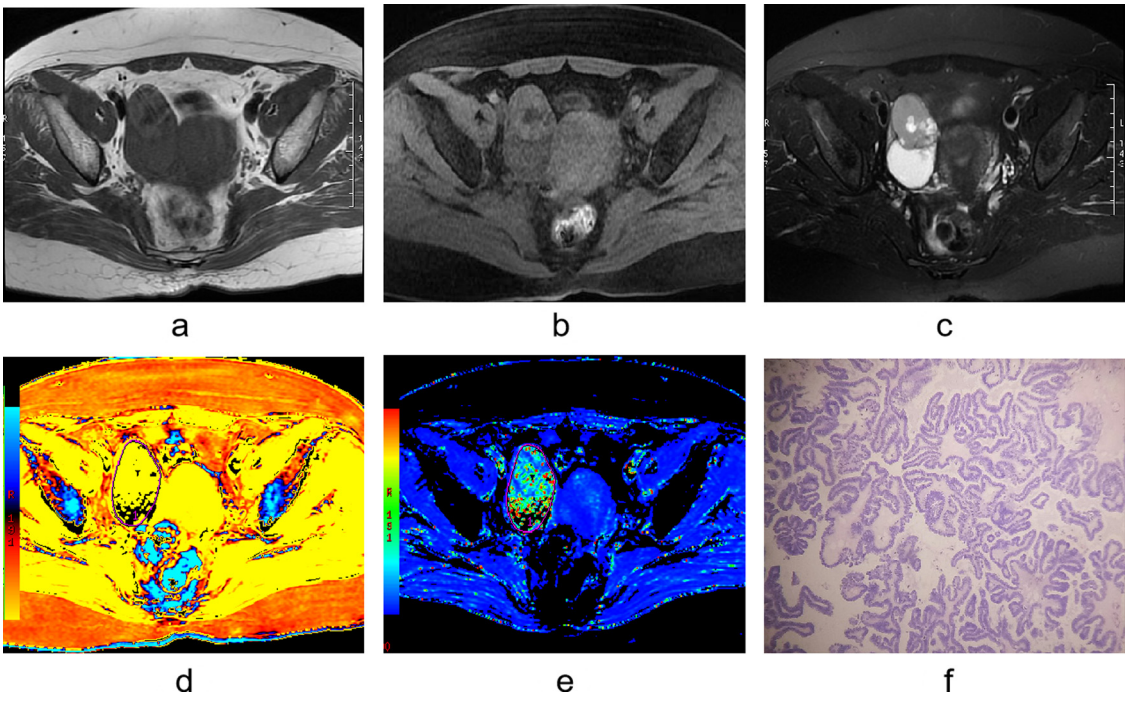


**Fig. 5.** A 51 years old female with right ovarian borderline serous papillary cystadenoma. $T_1$WI (a) and LAVA (b) shows a hypo-signal mass. (c) A fat suppression $T_2$WI shows hyper-signal. (d) $R_2$* map, $R_2$* value is 6.82 Hz. (e) $T_2$* map, $T_2$* value is 154.23 ms. (f) Pathological images (HE stain ×100) showed serous borderline papillary cystadenoma of the right ovary, with nuclear atypia, increased mitosis, branching papillary structures, and no stromal invasion.

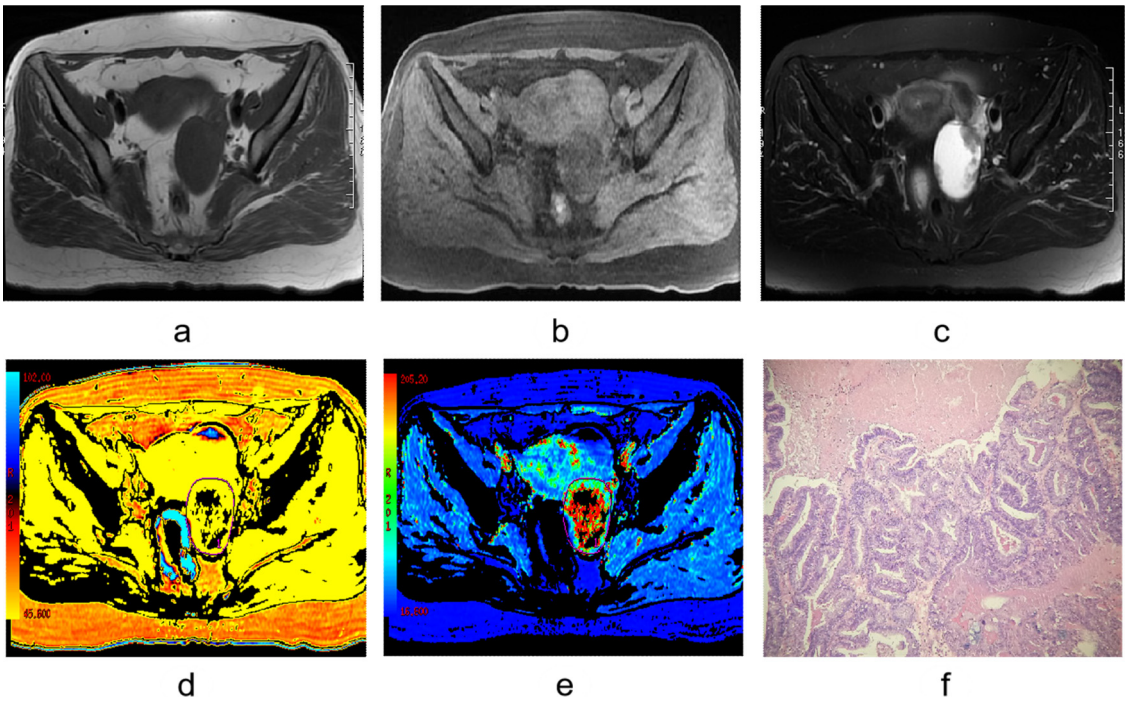


**Fig. 6.** A 57 years old female with left ovarian mucinous papillary cystadenocarcinoma. $T_1$WI (a) and LAVA (b) shows a hypo-signal mass. (c) A fat suppression $T_2$WI shows a hyper-signal mass with hypo-signal nodules. (d) $R_2$* map, $R_2$* value is 8.59 Hz. (e) $T_2$* map, $T_2$* value is 138.7 ms. (f) Pathological images (HE stain ×100) showed mucinous papillary cystadenocarcinoma of the left ovary with complex papillary structures and obvious nuclear atypia.

**Table 3**
The diagnostic performance of $R_2$* and $T_2$* values between BEOTs and MEOTs.

| | AUC | Cut-off | Sensibility | Specificity | Accuracy | PPV | NPV |
|---|---|---|---|---|---|---|---|
| $R_2$* | 0.894 | 7.50 Hz | 85.7% | 82.6% | 86.5% | 89.0% | 77.8% |
| $T_2$* | 0.776 | 143.73 ms | 71.4% | 82.6% | 78.4% | 87.1% | 63.7% |

The data with bigger ICC values were used for statistical analysis. The magnitude, phase, $R_2$* and $T_2$* values between BEOTs and MEOTs were compared using the independent-sample *t* test. The receiver operating characteristic (ROC) curve was used to evaluate the diagnostic performance of ESWAN parameters that revealed significant difference, and the areas under ROC curve (AUC) were provided. The corresponding sensitivity, specificity, accuracy, positive predictive value

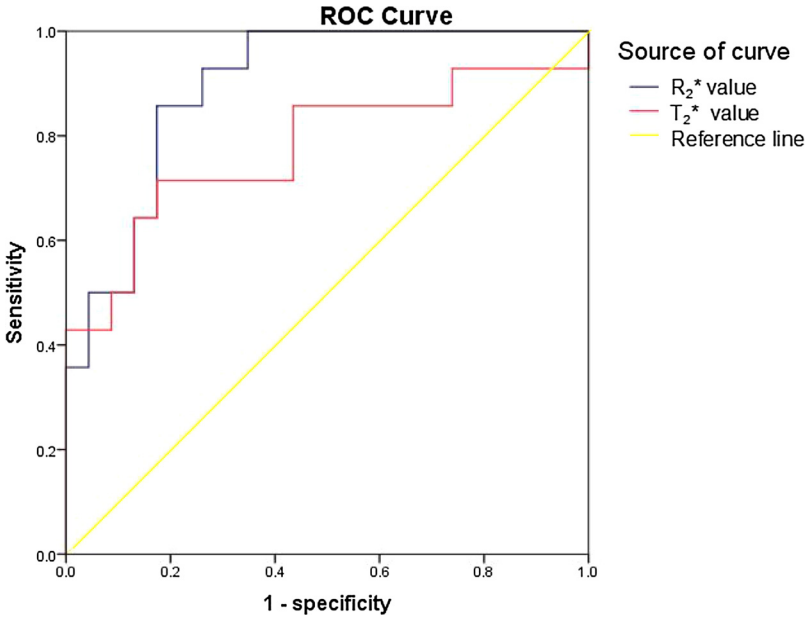


**Fig. 7.** ROC curves of $R_2$* and $T_2$* between BEOTs and MEOTs. AUC of R2* is 0.894 and AUC of $T_2$* is 0.776.

(PPV) and negative predictive value (NPV) were calculated at the optimal cutoff values.

## 3. Results

The ICC values of magnitude, phase, $R_2$* and $T_2$* values were all greater than 0.75 (Fig. 2). Furthermore, most data points were inside the 95% limits of agreement (LOA) between two observers (Fig. 3). Taken together, the obtained results indicated a good intra-observer and inter-observer agreement. The data with better intra-observer agreement were used for further analysis.

The differences in ESWAN parameters between BEOTs and MEOTs are shown in Table 2. Boxplots (Fig. 4) showed the magnitude, phase, $R_2$*, and $T_2$* values in BEOTs and MEOTs.

Comparison of ESWAN parameters between BEOTs and MEOTs are shown in Table 2. Compared with MEOTs, the $R_2$* value of BEOTs was significantly lower than that of MEOTs ([5.98 ± 1.79 vs. 11.40 ± 3.66] Hz; $t = -6.02$, $P < 0.001$), whereas the mean $T_2$* value of BEOTs was significantly higher than that of MEOTs ([187.91 ± 75.57 vs. 129.09 ± 28.48] ms; $t = 2.79$, $P = 0.01$),as shown in Fig. 5 and 6. The differences in magnitude values and phase values between BEOTs and MEOTs had no significant difference.

The AUC of $R_2$* values was 0.894 (95% confidence interval, CI:0.749–0.971) and the corresponding cutoff value was 7.50 Hz with a sensitivity, specificity and accuracy of 85.7%, 82.6% and 86.5%, respectively, and with a positive predictive value (PPV) and negative predictive value (NPV) of 89.0% and 77.8%, respectively. The AUC of $T_2$* values was 0.776 (95% CI:0.610–0.896) and the corresponding cutoff value was 143.73 ms with a sensitivity, specificity and accuracy of 71.4%, 82.6% and 78.4%, respectively, and with a PPV and NPV of 87.1% and 63.7%, respectively (Table 3). The ROC curves of $R_2$* and $T_2$* values in differentiating BEOTs from MEOTs are shown in Fig. 7.

## 4. Discussion

ESWAN, an SWI-like sequence,combines a novel 3D $T_2$* based multiecho acquisition with a special reconstruction algorithm. Compared with conventional SWI, ESWAN has significant advantages such as a strengthened susceptibility sensitivity, high signal-to-noise ratio (SNR), shorten scanning time, reduced image distortion [25,26]; and quantitative evaluation parameters (magnitude images, phase images, $R_2$* images and $T_2$* images) [27].

The magnitude maps mainly reflect the comparison of signal intensity between tissues, and contain abundantly comparative information from tissues, which can clearly show different organizational structures [28,29], whereas, the phase maps reflect the magnetic susceptibility differences in tissues, which are only related to the content of magnetic substances between tissues, and are independent of water content and proton density [29]. In this study, we showed that magnitude values had no difference between BEOTs and MEOTs, which was consistent with previous study [21] that examined the differences between prostate hyperplasia and prostate cancer using ESWAN. In addition, we showed that phase values did not differentiate between two groups of tumors. In contrast, Xin et al. [21] have reported higher phase values in the prostate hyperplasia group compared to prostatic cancer group. This difference is caused by the different ingredient in lesions and the different ROI selection. Previous study [21] has reported solid prostate lesions and circle ROIs, while in this study both tumor groups had predominantly cystic ingredient and the ROIs were generated using the maximum level method which can reduce the underestimation of tumor heterogeneity.

$R_2$* is transverse relaxation rate that is obtained via gradient reunion at different times. The $R_2$* value is directly related to the tissue deoxygenated hemoglobin concentration and can be used to quantitatively assess changes of oxygen content in local tissue [30,31]. A high $R_2$* value indicates a lower oxygen, an increase in deoxygenated hemoglobin, and a decrease in MR signal. $T_2$* is effective transverse relaxation time, which is obtained without removing the influence of magnetic field uniformity and surrounding magnetic materials. $T_2$* value is affected by content of paramagnetic substances [32], proton density, water content, and the motion state of water molecule. $T_2$* value is the reciprocal of $R_2$* value [31]. Our study indicated that the $R_2$* value of BEOTs was lower, while the $T_2$* value was higher compared to MEOTs. We hold the opinion that the results are closely related to oxygen consumption in different tissues and immature neovascularization. According to the histological analysis, MEOTs are more invasive and higher proliferation rate compared to BEOTs. In the cystic components, the MEOTs are characterized by more hemorrhage and necrosis. In the solid components, the MEOTs have an increased immature angiogenesis. Both above factors can reduce the oxygen saturation of MEOTs, but increase the concentrations of deoxyhemoglobin and hemosiderin. As the increasing of deoxyhemoglobin and

hemosiderin concentrations, the magnetic susceptibility differences of tumor are strengthen. MEOTs have stronger magnetic susceptibility than BEOTs, lead to an increase of $R_2$* value and a decrease of $T_2$* value. Furthermore, MEOTs have high cell density, where water molecules diffuse restriction, which also reduced the $T_2$* value of MEOTs. Our results were consistent with a study performed by Tian and his team [22] who used ESWAN sequences to identify cystic kidney cancer and complex renal cysts, and discovered that $R_2$* value of cystic renal cancer was higher than that of complex renal cyst. In addition, Tian and his team [23] have used $R_2$* value to evaluate the invasiveness of primary hepatocellular carcinoma, reporting that the $R_2$* value of the invasiveness group was higher compared to the non-invasiveness group, which suggested that $R_2$* can be used to effectively distinguish the invasiveness of primary hepatocellular carcinoma. This study suggested that $R_2$* and $T_2$* could be used to effectively distinguish between BEOTs and MEOTs, and specially R2* which had a better diagnostic performance with a sensitivity of 85.7%, specificity of 82.6%, and accuracy of 86.5%.

This study has some limitations that need to be pointed out. The sample size was small and needs to be expanded in the future study. In addition, it was not possible to compare different histological types and different FIGO stages. Furthermore, a manual ROI on maximal solid area slice or maximal slice in tumor was used for calculation; nevertheless, histogram analysis could be considered for differentiating the two groups of tumors in the future study. Histogram analysis is more sensitive method for reflecting more information of pathological changes and microstructural heterogeneity of the whole tumor, and reduce the underestimation of tumor heterogeneity.

## 5. Conclusion

MR-ESWAN does not require injected contrast, it can be used as a safe and effective method for differentiating BEOTs from MEOTs. The $R_2$* values have the better diagnostic performance compared to $T_2$*.

## Funding

This research did not receive any specific grant from funding agencies in the public, commercial, or not-for-profit sectors.

## Declaration of Competing Interest

The authors declare no conflicts of interest.

We declare that we do not have any commercial or associative interest that represents a conflict of interest in connection with the work submitted.

## References

[1] F. Zeppernick, I. Meinholdheerlein, The new FIGO staging system for ovarian, fallopian tube, and primary peritoneal cancer, Arch. Gynecol. Obstet. 290 (5) (2014) 839–842, https://doi.org/10.1007/s00404-014-3364-8.

[2] J. Prat, FIGO Committee on Gynecologic Oncology, FIGO's staging classification for cancer of the ovary, fallopian tube, and peritoneum: abridged republication, J. Gynecol. Oncol. 26 (2) (2015) 87–89, https://doi.org/10.3802/jgo.2015.26.2.87.

[3] S.J. Seong, D.H. Kim, M.K. Kim, T. Song, Controversies in borderline ovarian tumors, J. Gynecol. Oncol. 26 (4) (2015) 343–349, https://doi.org/10.3802/jgo.2015.26.4.343.

[4] C.L. Bent, A. Sahdev, A.G. Rockall, et al., MRI appearances of borderline ovarian tumours, Clin. Radiol. 64 (4) (2009) 430–438, https://doi.org/10.1016/j.crad.2008.09.011.

[5] P. Solmaz Hasdemir, T. Guvena, Borderline ovarian tumors" A contemporary review of clinicopathological characteristics, diagnostic methods and therapeutic options, J. BUON 21 (4) (2016) 780–786.

[6] J. Chen, C. Chang, H.C. Huang, et al., Differentiating between borderline and invasive malignancies in ovarian tumors using a multivariate logistic regression model, Taiwan. J. Obstet. Gynecol. 54 (4) (2015) 398–402, https://doi.org/10.1016/j.tjog.2014.02.004.

[7] L. Helpman, M.E. Beiner, S. Aviel-Ronen, et al., Safety of ovarian conservation and fertility preservation in advanced borderline ovarian tumors, Fertil. Steril. 104 (1) (2015) 138–144, https://doi.org/10.1016/j.fertnstert.2015.03.038.

[8] J. Prat, The results of conservative (fertility-sparing) treatment in borderline ovarian tumors vary depending on age and histological type, Ann. Oncol. 25 (7) (2014) 1255–1258, https://doi.org/10.1093/annonc/mdu160.

[9] M. Morotti, M.V. Menada, D.J. Gillott, P.L. Venturini, S. Ferrero, The preoperative diagnosis of borderline ovarian tumors: a review of current literature, Arch. Gynecol. Obstet. 285 (4) (2012) 1103–1112, https://doi.org/10.1007/s00404-011-2194-1.

[10] E. Kolwijck, C.M. Thomas, J. Bulten, L.F. Massuger, Preoperative CA-125 levels in 123 patients with borderline ovarian tumors: a retrospective analysis and review of the literature, Int. J. Gynecol. Cancer 19 (8) (2009) 1335–1338, https://doi.org/10.1111/IGC.0b013e3181a83e04.

[11] N. Bharwani, R.H. Reznek, A.G. Rockall, Ovarian Cancer Management: the role of imaging and diagnostic challenges, Eur. J. Radiol. 78 (1) (2011) 41–51, https://doi.org/10.1016/j.ejrad.2010.11.039.

[12] N.M. deSouza, R. O'Neill, G.A. McIndoe, R. Dina, W.P. Soutter, Borderline tumors of the ovary: CT and MRI features and tumor markers in differentiation from stage I disease, AJR Am. J. Roentgenol. 184 (3) (2005) 999–1003, https://doi.org/10.2214/ajr.184.3.01840999.

[13] M. Hori, H. Mori, S. Aoki, et al., Three-dimensional susceptibility-weighted imaging at 3 T using various image analysis methods in the estimation of grading intracranial gliomas, Magn. Reson. Imaging 28 (4) (2010) 594–598, https://doi.org/10.1016/j.mri.2010.01.002.

[14] V. Sehgal, Z. Delproposto, E.M. Haacke, et al., Clinical applications of neuroimaging with susceptibility-weighted imaging, J. Magn. Reson. Imaging 22 (4) (2005) 439–450, https://doi.org/10.1002/jmri.20404.

[15] Fang Ji, Wen Di, Tumor microenvironment affecting biological behaviour of malignant ovarian neoplasms: an update, J. Int. Obstet. Gyneeol. 39 (4) (2012) 352–355, https://doi.org/10.3969/j.issn.1674-1870.2012.04.010.

[16] G.L. Semenza, Hypoxia-inducible factor 1 and cancer pathogenesis, IUBMB Life 60 (9) (2008) 591–597, https://doi.org/10.1002/iub.93.

[17] A. Giatromanolaki, E. Sivridis, M.I. Koukourakis, Tumour angiogenesis: vascular growth and survival, APMIS 112 (7–8) (2004) 431–440, https://doi.org/10.1111/j.1600-0463.2004.apm11207-0804.x.

[18] G. Sparacia, C. Speciale, A. Banco, F. Bencivinni, M. Midiri, Accuracy of SWI sequences compared to T2*-weighted gradient echo sequences in the detection of cerebral cavernous malformations in the familial form, Neuroradiol. J. 29 (5) (2016) 326–335, https://doi.org/10.1177/1971400916665376.

[19] J.J. Tao, W.J. Zhang, D. Wang, et al., Susceptibility weighted imaging in the evaluation of hemorrhagic diffuse axonal injury, Neural Regen. Res. 10 (11) (2015) 1879–1881, https://doi.org/10.4103/1673-5374.170322.

[20] C. Zeng, S. Du, Y. Han, et al., Optic radiations are thinner and show signs of iron deposition in patients with long-standing remitting-relapsing multiple sclerosis: an enhanced T2*-weighted angiography imaging study, Eur. Radiol. 28 (10) (2018) 4447–4454, https://doi.org/10.1007/s00330-018-5461-8.

[21] J.Y. Xin, S.S. Gao, J.G. Liu, et al., The value of ESWAN in diagnosis and differential diagnosis of prostate cancer: preliminary study, Magn. Reson. Imaging 44 (2017) 26–31, https://doi.org/10.1016/j.mri.2017.08.002.

[22] S.F. Tian, A.L. Liu, Y. Li, et al., The value of MR magnetic sensitive technology to identify the cystic renal cell carcinoma and complex renal cysts, Chin. J. Magn. Reson. Imaging 6 (10) (2015) 762–767, https://doi.org/10.3969/j.issn.1674-8034.2015.10.009.

[23] S.F. Tian, A.L. Liu, J.H. Liu, et al., Value of R2(*) in evaluating the biological behavior of primary hepatocellular carcinoma, Zhonghua Yi Xue Za Zhi 96 (15) (2016) 1164–1167, https://doi.org/10.3760/cma.j.issn.0376-2491.2016.15.004.

[24] Y. Li, Q.W. Song, M.Y. Sun, et al., Use of enhanced T2 star-weighted angiography (ESWAN) and R2* values to distinguish ovarian cysts due to endometriosis from other causes, Abdom. Imaging 40 (6) (2015) 1733–1741, https://doi.org/10.1007/s00261-014-0314-7.

[25] L.F. Guo, G. Wang, X.Y. Zhu, C. Liu, L. Cui, Comparison of ESWAN, SWI-SPGR, and 2D T2*-weighted GRE sequence for depicting cerebral microbleeds, Clin. Neuroradiol. 23 (2) (2013) 121–127, https://doi.org/10.1007/s00062-012-0185-7.

[26] C. Denk, A. Rauscher, Susceptibility weighted imaging with multiple echoes, J. Magn. Reson. Imaging 31 (1) (2010) 185–191, https://doi.org/10.1002/jmri.21995.

[27] X. Ling, W. Tang, G. Liu, et al., Assessment of brain maturation in the preterm infants using diffusion tensor imaging (DTI) and enhanced T2 star weighted angiography (ESWAN), Eur. J. Radiol. 82 (9) (2013) e476–e483, https://doi.org/10.1016/j.ejrad.2013.04.003.

[28] Jianying Xin, Xianmin Shao, Shanshan Gao, et al., Comparative study of ESWAN imaging and clinical indexes of benign prostate hyperplasia, J. Clin. Interv. Radiol. ISVIR 35 (2) (2016) 238–242, https://doi.org/10.13437/j.cnki.jcr.2016.02.022.

[29] Huipeng Ren, Lei Zhang, Zhuqin Ren, et al., Value of contrast measurement of ESWAN-R2* value in diagnosis of neonatal punctate white matter lesions, Chin. J. Magn. Reson. Imaging 4 (3) (2013) 201–205, https://doi.org/10.3969/j.issn.1674-8034.2013.03.008.

[30] Xiaodan Liu, Ying Wang, Xueying Ling, Li Huang, The study of ESWAN in vascular cognitive Impairment-No dementia with small vessel disease, J. Clin. Interv. Radiol. ISVIR 31 (8) (2012) 1064–1071, https://doi.org/10.13437/j.cnki.jcr.2012.08.034.

[31] S. Chopra, W.D. Foltz, M.F. Milosevic, et al., Comparing oxygen-sensitive MRI (BOLD R2*) with oxygen electrode measurements: a pilot study in men with prostate cancer, Int. J. Radiat. Biol. 85 (9) (2009) 805–813, https://doi.org/10.1080/09553000903043059.

[32] T. Christen, B. Lemasson, N. Pannetier, et al., Is T2* enough to assess oxygenation? Quantitative blood oxygen level–dependent analysis in brain tumor, Radiology 262 (2) (2012) 495–502, https://doi.org/10.1148/radiol.11110518.